Complete characterization of a Yb-based OPA at a high repetition rate using frequency resolved optical switching

Elissa Haddad, Adrien Longa, Philippe Lassonde, Adrien Leblanc, Heide Ibrahim, Fabio Boschini, François Légaré, Gaëtan Jargot

Research Article | Vol. 31, No. 16 / 31 Jul 2023 / Optics Express 25840
Optics EXPRESS

Complete characterization of a Yb-based OPA at a high repetition rate using frequency resolved optical switching

Elissa Haddad,[1,3,†] Adrien Longa,[1,†] Philippe Lassonde,[1] Adrien Leblanc,[2] Heide Ibrahim,[1] Fabio Boschini,[1] François Légaré,[1,*] and Gaëtan Jargot[1]

[1]Advanced Laser Light Source (ALLS) at Centre Énergie Matériaux Télécommunications, Institut national de la recherche scientifique, 1650 Boulevard Lionel-Boulet, Varennes, Québec J3X 1P7, Canada
[2]Laboratoire d'Optique Appliquée, École Polytechnique, ENSTA, CNRS, Université Paris Saclay, Palaiseau, France
[3]elissa.haddad@inrs.ca
[†]These authors contributed equally to this work.
[*]francois.legare@inrs.ca

Abstract: We demonstrate experimentally that frequency resolved optical switching (FROSt) can be used to characterize ultra-broadband pulses at high repetition rates up to 500 kHz. Specifically, we present the complete temporal characterization of an optical parametric amplifier (OPA), from the supercontinuum (SC) to the second stage of amplification. Simultaneous characterization of co-propagating signal and idler pulses enables retrieval of their group delay, as well as their temporal phase and intensity. Our study focuses on an extensive frequency range spanning the infrared region (1.2 to 2.4 µm) and confirms the strength and convenience of FROSt as a single tool for characterizing a wide range of pulses at high repetition rates.

1. Introduction

Over recent years, major developments have resulted in advanced high repetition rate laser sources based on the ytterbium (Yb) gain media. Different Yb-based technologies have emerged such as thin-disk, InnoSlab, and fiber lasers [1–3] which are crucial for a wide range of applications (scientific and industrial), e.g. increasing the flux of extreme ultraviolet (EUV) and soft X-ray radiations from the process of high harmonic generation [4,5] and accessing attosecond pulse duration [6]. Yb lasers have the advantage to provide up to kilowatts of average power, paving the way to the third-generation femtosecond technology [7]. In contrast, the titanium-sapphire (Ti:Sa) technology is limited to ~20 W of average power (e.g. 10 kHz, 2 mJ). However, Ti:Sa lasers can provide ~40-fs pulses, while Yb-based lasers tend to have longer pulse durations (250 fs to 1 ps). Indeed, they require higher compression factors to reach few-cycle pulse duration.

Yttberbium technology, combined with optical parametric amplification, has led to the development of high-repetition rate optical parametric chirped-pulse amplifiers (OPCPA) [8,9] that achieve unprecedented peak power at high average power for tabletop systems. Major efforts have been made to reach the mid-infrared (MIR) spectral range [10–13], which is of great importance for experimental investigations in strong-field physics that are currently carried out at lower repetition rate, including time- and angle-resolved photoemission spectroscopy (TR-ARPES) [14–17], cold target recoil-ion momentum spectroscopy (COLTRIMS) [18,19], Coulomb explosion imaging (CEI) [20,21], and high harmonic generation (HHG) [22,23]. Nevertheless, characterizing such systems with ultrashort and broadband pulses at high repetition rate remains a challenging and intricate task.

#494658 https://doi.org/10.1364/OE.494658
Journal © 2023 Received 5 May 2023; revised 8 Jun 2023; accepted 10 Jun 2023; published 19 Jul 2023

Optics EXPRESS

The characterization and control of the spectral phase of such short pulses is a key step in the progress of the above-mentioned techniques. In fact, the spectral phase directly impacts the temporal shape of the pulse, and its control enables access to higher peak power. For most Yb-based optical parametric amplifier (OPA) systems, only the output signal and idler are characterized using well-established techniques such as dispersion scan (D-scan) [24,25] or frequency resolved optical gating (FROG) [8,10]. This is primarily because the low energy at the supercontinuum (SC) stage presents a major technical challenge. Yet, the characterization of the SC grants a thorough control of the dispersion across all OPA stages, thus ensuring a higher efficiency.

In this work, we present a complete characterization of an Yb-based OPA using frequency resolved optical switching (FROSt). Our characterization spans from the supercontinuum pulses to the simultaneous characterization of the signal and idler output pulses. We also investigated the relaxation dynamics of silicon (Si) – the semiconductor used throughout these FROSt experiments – to estimate the repetition rate at which FROSt can still work for the current setup conditions. The relaxation time of photoexcited semiconductors is a complex phenomenon that depends on multiple parameters and can vary from nanoseconds to microseconds [26–28].

Based on transient absorption in solids, the FROSt technique is free of phase-matching constraints (i.e. nonlinear conversion is not required) and polarization-independent [29,30]. By using a pump pulse to switch the optical transmission of a solid, FROSt allows the characterization of a pulse (the probe) by analyzing its resulting transmission through the material as a function of pump-probe time delay. In principle, FROSt is spectrally limited only by the sensitivity of the spectrometer and the transparency range of the material used to perform the measurement. It enables the characterization of multi-octave pulses [31] and simultaneous characterization of pulses with different polarizations [32]. As previously mentioned, the FROSt technique relies on the use of a pump pulse to switch the optical transmission of a solid, and this pump must be synchronized with the probe beam being characterized. While this requirement may be a drawback in certain configurations, it is worth noting that in the case of an OPA, the pump and seed beams are synchronized throughout the amplification process, making the implementation of the FROSt technique straightforward. FROSt was first demonstrated at low repetition rates with Ti:Sa technology. The aim of this study is to demonstrate that FROSt works even at high repetition rate, up to 500 kHz, to precisely characterize ultrashort few-cycle pulses from an Yb-based OPA system.

2. Methods

All the experiments were performed at the Advanced Laser Light Source (ALLS) user facility, using an industrial-grade Yb-doped fiber amplifier laser (Tangerine, Amplitude). This laser delivers pulses around 150-fs duration with 200 μJ per pulse for a maximum average power of 50 W (at a repetition rate of 250 kHz). A controllable grating inside the laser allows the user to change the pulse duration. The repetition rate of the laser is also adjustable from few Hz up to 2 MHz.

In the near future, this laser will be used to generate ultrashort tunable light pulses to perform TR-ARPES measurements. Hence, this source is divided into two beamlines. One beam will be used to derive a probe in the EUV region (i.e. 6 eV up to 42 eV) and the second beam will serve as a pump for an ultrashort tunable OPA in the MIR region (i.e. 4 to 8 μm). These amplified pulses will then be employed to photoexcite a wide variety of quantum materials, spanning from topologically-protected systems to unconventional superconductors. For this reason, we use a beam splitter (BS) with 75 % transmission and 25 % reflection at the output of the laser, as shown on the left in Fig. 1.

Our approach to reach the MIR region involves a commonly used scheme of difference frequency generation (DFG) between the signal and idler at the output of an OPA. Both of these

Optics EXPRESS

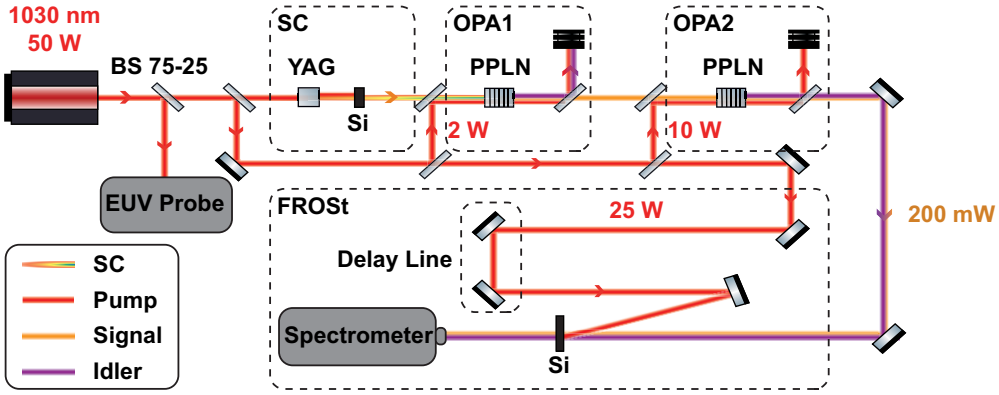

Fig. 1. Schematic of the experimental setup of the two-stage OPA (from left to right) followed by the FROSt (bottom) implemented to characterize the signal and the idler. Starting from the left, the Yb laser output is separated into two beams with a beam splitter (BS 75-25). The reflected beam will be an EUV probe. The transmitted beam is used to generate a supercontinuum (SC). That SC goes through a MgO:PPLN crystal in the first-stage OPA (OPA1) and the output signal is amplified in another MgO:PPLN in the second-stage OPA (OPA2). The idler generated in this process is kept. For the FROSt, the collinear signal and idler transmitted through a Si sample are collected in a spectrometer. The FROSt pump beam is picked up after the initial BS 75-25 and focused on the Si sample after going through a delay line.

beams are in the short wavelength infrared (SWIR) range, with wavelengths between 1.75 and 2.45 μm. The focus of this work is to characterize the signal and idler to enhance conversion efficiency towards longer wavelengths.

Throughout this work, the Yb-based laser is chirped to 300 fs, which has been determined experimentally to be the optimal duration in our conditions to maximize the conversion of the pump into the signal and idler. The experimental setup is depicted in Fig. 1. The seed is generated in a 10-mm-long YAG crystal through white light generation (WLG) by tightly focusing few microjoules of the pump laser. A wide spectrum from the visible to the SWIR – the supercontinuum (SC) – is generated. The bandwidth of interest is between 1750 nm and 1950 nm. The seed is then stretched in time with a 2-mm-thick Si plate in order to reach the best trade-off between gain and bandwidth in the first amplification stage (see SC in Fig. 1). Both stages of amplification (OPA1 and OPA2 in Fig. 1) are in collinear geometry and are identically composed of 1-mm-long MgO:Periodically Poled Lithium Niobate (PPLN) crystals with 10 discrete periods from 27.58 to 31.59 μm along the transverse direction of the crystal. The most efficient period is chosen according to the wavelength to amplify by translating the crystal in the transverse direction of the pump beam. 8 μJ are used to pump the first stage, and the pump and the idler produced during the amplification stage are dumped. The signal is refocused, and 25 μJ are used to pump the second amplification stage, resulting in a total of 200 mW for the signal and idler combined.

Using the FROSt technique, we characterize three components of the OPA: the seed generated via SC as well as the amplified signal and idler. The SC beam is characterized first. The collinear signal and idler are simultaneously characterized at the output of the two amplification stages. The implementation of the FROSt measurement is the same for all the beams to be characterized [29] and is depicted in Fig. 1, in the FROSt frame. The remaining pump is delayed to temporally and spatially overlap with the probe onto a Si plate of 0.5 mm. We purposely used Si as a medium for our FROSt measurements because of its 1.12 eV bandgap, which is below the pump photon

Optics EXPRESS

energy (1.2 eV), and it has a good transmission up to 6.5 μm. The beam is subsequently collected into a spectrometer (NIRQuest+2.5, Ocean Insight) to acquire the FROSt spectrogram.

3. Semiconductor relaxation dynamics

When looking at the way FROSt works, the element that could potentially limit the maximum achievable repetition rate is the semiconductor material. Even if the pump fluence is high enough to photoexcite the material, the pulse-to-pulse interval must be sufficiently long to allow the sample to relax and thus the transmission to recover to obtain exploitable spectrograms, without pulse-to-pulse cumulative effects.

In an effort to find the maximum possible repetition rate for FROSt measurements, we performed a simplified pump-probe experiment to extract the relaxation time of the Si sample used for the pulse characterization technique, under the FROSt conditions.

We focused on the relaxation time of silicon here because it is the ideal switch material for our experiment as mentioned previously. Since we expect the timescale of the relaxation dynamics to be in the range of tens of nanoseconds to tens of microseconds [26–28], photodiodes are sufficiently fast for such measurements. It is important to note that the free carrier lifetime in semiconductors depends on several parameters, including material quality, sample thickness, as well as excitation wavelength and fluence [33–35]. The goal of our experiment is simply to estimate the relaxation time of our sample under the FROSt conditions.

In practice, we used a commercial continuous-wave (CW) laser diode centered at 1550 nm that we focused to probe the semiconductor sample – the same 0.5-mm-thick Si wafer used for all measurements. 40-fs pulses centered at 800 nm delivered by a 50 Hz Ti:Sa laser system were used to pump the Si sample, thus inducing the ultrafast switch of the material. Measurements were performed for different pump energies while keeping the same pump spot size to observe the effect of changing pump fluence. The spot size of the pump laser beam was more than twice that of the probe to ensure uniform excitation of the material in the probed area. The probe transmission through the switch was monitored using an InGaAs detector (DET10D2 Thorlabs photodiode) with a ~25 ns rise time. A mechanical laser shutter (Uniblitz) was placed in the pump beam path to isolate single pulses, thus ensuring that the sample was always at its equilibrium state for each measurement.

The data was acquired over a timeframe of hundreds of microseconds by connecting the photodiode to a digital oscilloscope (Tektronix TDS5054B) and synchronizing the acquisition with the arrival of the pump pulse using a trigger.

Figure 2 shows the intensity of the transmitted probe on the photodiode as a function of time (red curve) when the sample is pumped with 750 μJ pulses. Time zero coincides with the moment the pump pulse reaches the sample, where we observe an abrupt decrease of the transmissivity. Yet, the transmission drop does not represent the true timescale of the physical phenomena since the photodiode response time is too slow. The recovery part we are interested in, however, corresponds to the real dynamics as it is much slower. The recovery curve was fitted with a bi-exponential function (black dashed line) and a relaxation time (at $1/e^2$) of ~4 μs was obtained. The inset of Fig. 2 presents the zoomed-in transmission curve for 750-μJ pump pulses in red, along with the curves for different pump energies – 125 μJ, 250 μJ, and 500 μJ, respectively in yellow, blue, and green. As expected, the relaxation time slightly increases with fluence, from 1 μs to 4 μs.

These results highlight the trade-off between fluence and repetition rate for FROSt measurements. Fluence must be increased to sufficiently reduce transmission and obtain a good contrast in the FROSt spectrograms. However, at higher fluences, the relaxation time of Si increases, limiting the repetition rate we can measure. Based on these initial findings, we anticipate that the maximum possible repetition rate to measure FROSt spectrograms will be between 250 kHz and 1 MHz, which correspond to pulse-to-pulse intervals between 4 μs and 1 μs.

Optics EXPRESS

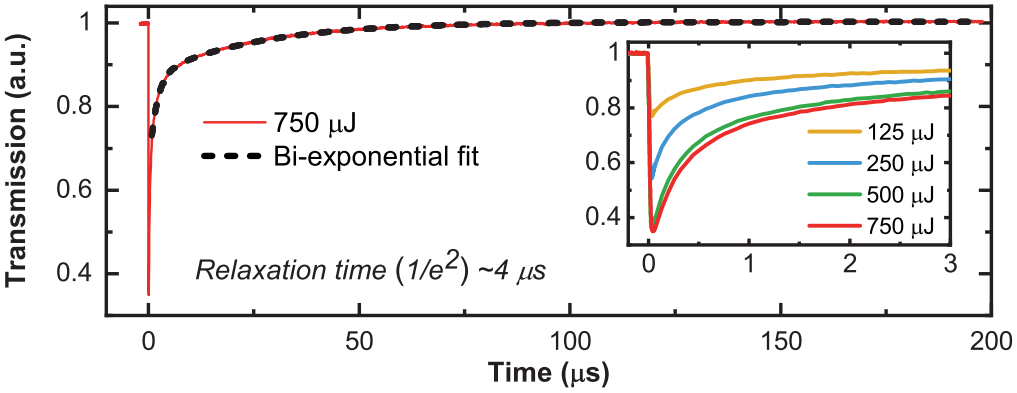

Fig. 2. Relaxation time of silicon: transmission curve of the probe as a function of delay following photoexcitation from a 750-μJ pump and bi-exponential curve fit. The inset shows the zoomed-in relaxation curves of Si for different pump energies.

4. Supercontinuum characterization

We first characterized the OPA SC seed pulses using the FROSt technique described previously. Characterizing such low energy broadband pulses is tedious using other conventional pulse characterization techniques. Thanks to the energy tunability of the Yb laser, we were able to generate and characterize pulses at 50 kHz, 250 kHz, and 500 kHz at energies down to nanojoules. We managed to perform FROSt measurements up to 500 kHz, which is in the expected threshold range determined from the Si relaxation time. Figure 3(a) shows the experimental FROSt spectrogram obtained at the maximum repetition rate of 500 kHz for the nanojoule supercontinuum pulses extending from 1.2 to 1.8 μm. Negative delays correspond to the time before the pump reaches the semiconductor sample. The ~23% contrast between the transmitted signal before and after the pump is quite low in Fig. 3(a), but still sufficient for the ptychographic pulse retrieval algorithm used to converge [29]. The numerically retrieved spectrogram is illustrated in Fig. 3(b) and reproduces all the essential features of the measured FROSt trace. Figures 3(c) and 3(d) show the intensity (red line) and phase (green line) of the reconstructed spectrum and temporal pulse, respectively. We obtain a pulse duration of ~18 fs (FWHM) with significant third-order dispersion [36].

We attempted FROSt characterization of pulses above 500 kHz repetition rate, but the absorption contrast in the spectrogram decreased significantly, making it impossible to reconstruct the traces. In other words, when measuring the transmitted spectrum at negative delays, before the pump pulse supposedly reached the sample, residual effects from previous pump pulses were sizable. As discussed in the above section, even if the pump fluence is high enough to photoexcite the sample, the pulse-to-pulse interval must be sufficiently long to allow the sample to relax and thus the transmission to recover.

It is noteworthy that the contrast between the transmitted signal before and after the pump was lower than expected for all the spectrograms measured. Even at 50 kHz, the impact of consecutive pulses on the measurements is still noticeable, leading to a decrease in contrast. One hypothesis is that this could be due to the incubation effect, where the material accumulates some laser energy with each pulse instead of dissipating it completely. This mechanism has been extensively studied in metals and semiconductors for laser ablation, yet there is no consensus on the exact physical processes involved [37–40]. These effects take place even when the delay between consecutive laser pulses is longer than the thermal diffusion time, which could explain why there is a reduced contrast even at 50 kHz repetition rate.

Optics EXPRESS

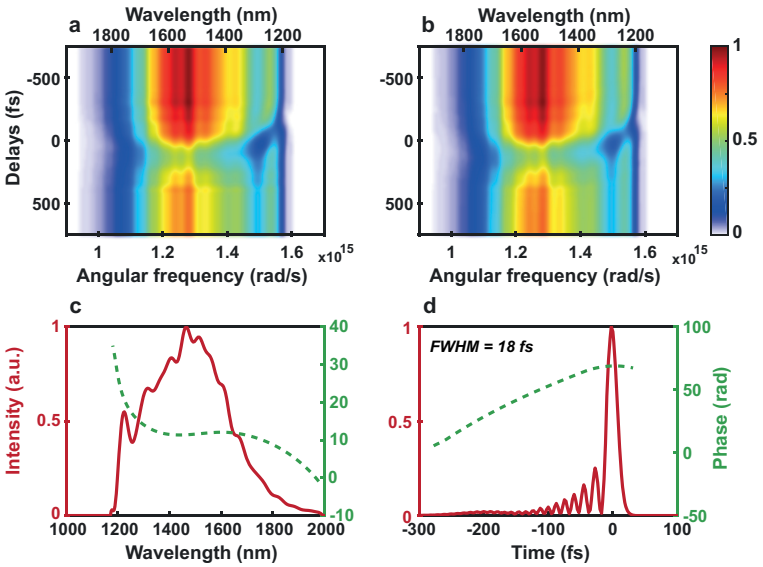

Fig. 3. FROSt characterization at 500 kHz of nanojoule broadband SC pulses centered at 1.5 μm. (a) Experimental FROSt trace, (b) retrieved FROSt trace, and retrieved pulse intensity (red) and phase (green) (c) in the spectral domain and (d) in the temporal domain.

5. Signal and idler characterization

To complete the characterization of the home-built OPA, we measured simultaneously the collinear signal and idler output at 250 kHz after two amplification stages seeded by the supercontinuum (see OPA2 and FROSt in Fig. 1). This OPA is designed to work at 250 kHz, and any change in the repetition rate would affect thermal dynamics in the system and considerably reduce the efficiency. For this reason, all measurements for the signal and the idler were done at 250 kHz. In Fig. 4, we show the results obtained for two signal-idler pairs, respectively (I) 1.78 μm-2.36 μm, plotted in orange, and (II) 1.9 μm-2.25 μm, plotted in blue. Figures 4(a) and 4(c) present the experimental FROSt traces measured for pair I and pair II, respectively. The group delay between the generated signal and idler can be inferred from the FROSt spectrograms, as the spectral transmission drop does not occur at the same time for both pulses. This delay is related to the wavelength-dependent group velocity in nonlinear crystals. Hence, as observed in Fig. 4, the delay between the signal and idler pulses is smaller for signal-idler pair II compared to I, because the signal and idler wavelengths are closer.

The corresponding retrieved FROSt traces are shown in Figs. 4(b) and 4(d). Both signal and idler pulses are retrieved simultaneously using a ptychographic algorithm [29]. Figure 4(e) highlights the spectral tunability of the OPA source in the SWIR, with the spectra calibrated according to the measured power for each central wavelength. All the retrieved spectral phases are also displayed on Fig. 4(e) in dotted lines. Figure 4(f) shows the retrieved intensity profile (solid line) and phase (dotted line) of the corresponding signal-idler pairs with both signal pulses, at 1.78 μm (in orange) and 1.9 μm (in blue), centered at 0 fs. The exact temporal delay between the signal and idler is also retrieved. For visualization purposes, the intensity of both idler pulses is multiplied by a factor 4. The duration measured and the Fourier transform limit (FTL) calculated for each pulse are listed in Table 1.

Optics EXPRESS

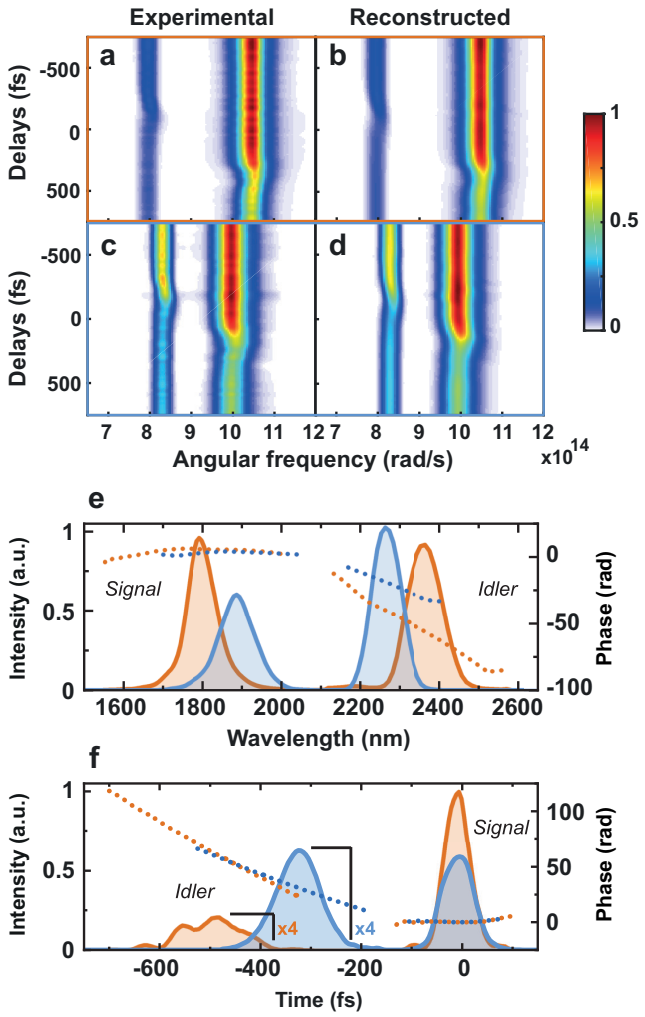

Fig. 4. FROSt characterization of two signal-idler pairs, I (in orange) and II (in blue), at 250 kHz. (a) Experimental and (b) retrieved FROSt trace of signal-idler I. (c) Experimental and (d) retrieved FROSt trace of signal-idler II. (e) Retrieved spectral phase and intensity and (f) temporal phase (dotted lines) and intensity (solid lines) for both signal-idler pair pulses.

Table 1. Pulse duration of each signal and idler pulse with the corresponding Fourier transform limit (FTL)

	Wavelength (μm)	Pulse duration (fs)	FTL (fs)
Signal	1.78	60	48
	1.9	78	60
Idler	2.36	108	80
	2.25	106	85

Optics EXPRESS

6. Conclusion

To conclude, we have demonstrated that the FROSt technique can be extended to characterize laser sources at high repetition rates, up to 500 kHz. The free carrier relaxation time of the semiconductor used for FROSt, in the range of 1 µs to 4 µs for silicon, limits the maximum repetition rate we can reach. Above 500 kHz, the transmission contrast in the spectrogram was not sufficient for our pulse retrieval algorithm to converge. Advances in materials science make it possible to reduce the relaxation time of materials and could potentially enable the use of the FROSt technique at even higher repetition rates through the development of short-carrier-lifetime semiconductors [33,34] or using higher purity materials [35].

We have presented the first instance of full temporal and spectral characterization of an OPA from the supercontinuum to the second stage of amplification. The supercontinuum characterized extended from 1.2 µm to 1.8 µm and we measured a pulse duration of ~18 fs. The signal and idler generated in the second stage of amplification were also characterized between 1.78 µm and 1.9 µm for the signal, and 2.25 µm and 2.36 µm for the idler.

The integration of this characterization technique into certain commercial OPCPA systems, given their intrinsic pump-probe synchronization, could enable real-time monitoring of the pulse duration, providing an important diagnostic tool. Furthermore, certain OPCPAs incorporate a pulse shaper or an acousto-optic programmable dispersive filter to adjust the spectral phase, and the addition of FROSt to this setup could enable to fine-tune and customize the control of the spectral phase.

In addition, the FROSt technique can be used in the MIR range [29], even at low signal energy, which is crucial for high repetition rate experimental studies in strong-field physics, including high harmonic generation, TR-ARPES, and COLTRIMS, that require precise control over spectral phase and pulse duration.

Funding. Ministère de l'Économie, de l'Innovation et de l'Énergie - Québec; PROMPT - Québec; Canada Foundation for Innovation; Fonds de recherche du Québec – Nature et technologies; Natural Sciences and Engineering Research Council of Canada.

Acknowledgments. We thank Antoine Laramée for his technical support in the laboratory. E. Haddad acknowledges financial support from NSERC Ph.D. scholarship program.

Disclosures. The authors declare no conflicts of interest.

Data availability. Data underlying the results presented in this paper are available upon reasonable request to the authors.

References

1. H. Lim, F. Ö. Ilday, and F. W. Wise, "Femtosecond ytterbium fiber laser with photonic crystal fiber for dispersion control," Opt. Express **10**(25), 1497–1502 (2002).
2. T. Nubbemeyer, M. Kaumanns, M. Ueffing, M. Gorjan, A. Alismail, H. Fattahi, J. Brons, O. Pronin, H. G. Barros, Z. Major, T. Metzger, D. Sutter, and F. Krausz, "1 kW, 200 mJ picosecond thin-disk laser system," Opt. Lett. **42**(7), 1381–1384 (2017).
3. B. E. Schmidt, A. Hage, T. Mans, F. Légaré, and H. J. Wörner, "Highly stable, 54mJ Yb-InnoSlab laser platform at 0.5kW average power," Opt. Express **25**(15), 17549–17555 (2017).
4. K. Midorikawa, "Progress on table-top isolated attosecond light sources," Nat. Photonics **16**(4), 267–278 (2022).
5. P.-A. Chevreuil, F. Brunner, S. Hrisafov, J. Pupeikis, C. R. Phillips, U. Keller, and L. Gallmann, "Water-window high harmonic generation with 0.8-µm and 2.2-µm OPCPAs at 100 kHz," Opt. Express **29**(21), 32996–33008 (2021).
6. M. Krebs, S. Hädrich, S. Demmler, J. Rothhardt, A. Zaïr, L. Chipperfield, J. Limpert, and A. Tünnermann, "Towards isolated attosecond pulses at megahertz repetition rates," Nat. Photonics **7**(7), 555–559 (2013).
7. H. Fattahi, H. G. Barros, and M. Gorjan, *et al.*, "Third-generation femtosecond technology," Optica **1**(1), 45–63 (2014).
8. M. Puppin, Y. Deng, O. Prochnow, J. Ahrens, T. Binhammer, U. Morgner, M. Krenz, M. Wolf, and R. Ernstorfer, "500 kHz OPCPA delivering tunable sub-20 fs pulses with 15 W average power based on an all-ytterbium laser," Opt. Express **23**(2), 1491–1497 (2015).
9. M. K. R. Windeler, K. Mecseki, A. Miahnahri, J. S. Robinson, J. M. Fraser, A. R. Fry, and F. Tavella, "100 W high-repetition-rate near-infrared optical parametric chirped pulse amplifier," Opt. Lett. **44**(17), 4287–4290 (2019).

Optics EXPRESS

10. N. Thiré, R. Maksimenka, B. Kiss, C. Ferchaud, G. Gitzinger, T. Pinoteau, H. Jousselin, S. Jarosch, P. Bizouard, V. Di Pietro, E. Cormier, K. Osvay, and N. Forget, "Highly stable, 15 W, few-cycle, 65 mrad CEP-noise mid-IR OPCPA for statistical physics," Opt. Express **26**(21), 26907–26915 (2018).
11. X. Zou, W. Li, S. Qu, K. Liu, H. Li, Q. J. Wang, Y. Zhang, and H. Liang, "Flat-Top Pumped Multi-Millijoule Mid-Infrared Parametric Chirped-Pulse Amplifier at 10 kHz Repetition Rate," Laser Photonics Rev. **15**, 2000292 (2021).
12. M. Mero, Z. Heiner, V. Petrov, H. Rottke, F. Branchi, G. M. Thomas, and M. J. J. Vrakking, "43 W, 1.55 µm and 12.5 W, 3.1 µm dual-beam, sub-10 cycle, 100 kHz optical parametric chirped pulse amplifier," Opt. Lett. **43**(21), 5246–5249 (2018).
13. P. Rigaud, A. Van de Walle, M. Hanna, N. Forget, F. Guichard, Y. Zaouter, K. Guesmi, F. Druon, and P. Georges, "Supercontinuum-seeded few-cycle mid-infrared OPCPA system," Opt. Express **24**(23), 26494–26502 (2016).
14. Y. H. Wang, H. Steinberg, P. Jarillo-Herrero, and N. Gedik, "Observation of Floquet-Bloch States on the Surface of a Topological Insulator," Science **342**(6157), 453–457 (2013).
15. I. Gierz, J. C. Petersen, M. Mitrano, C. Cacho, I. C. E. Turcu, E. Springate, A. Stöhr, A. Köhler, U. Starke, and A. Cavalleri, "Snapshots of non-equilibrium Dirac carrier distributions in graphene," Nat. Mater. **12**(12), 1119–1124 (2013).
16. M. Chávez-Cervantes, G. E. Topp, S. Aeschlimann, R. Krause, S. A. Sato, M. A. Sentef, and I. Gierz, "Charge Density Wave Melting in One-Dimensional Wires with Femtosecond Subgap Excitation," Phys. Rev. Lett. **123**(3), 036405 (2019).
17. S. Zhou, C. Bao, B. Fan, H. Zhou, Q. Gao, H. Zhong, T. Lin, H. Liu, P. Yu, P. Tang, S. Meng, W. Duan, and S. Zhou, "Pseudospin-selective Floquet band engineering in black phosphorus," Nature **614**(7946), 75–80 (2023).
18. R. Dörner, V. Mergel, O. Jagutzki, L. Spielberger, J. Ullrich, R. Moshammer, and H. Schmidt-Böcking, "Cold Target Recoil Ion Momentum Spectroscopy: a 'momentum microscope' to view atomic collision dynamics," Phys. Rep. **330**(2-3), 95–192 (2000).
19. H. Schmidt-Böcking, J. Ullrich, R. Dörner, and C. L. Cocke, "The COLTRIMS Reaction Microscope–The Spyhole into the Ultrafast Entangled Dynamics of Atomic and Molecular Systems," Ann. Phys. **533**, 2100134 (2021).
20. H. Ibrahim, B. Wales, S. Beaulieu, B. E. Schmidt, N. Thiré, E. P. Fowe, C. T. Hebeisen, V. Wanie, M. Giguére, J.-C. Kieffer, M. Spanner, A. D. Bandrauk, J. Sanderson, M. S. Schuurman, and F. Légaré, "Tabletop imaging of structural evolutions in chemical reactions demonstrated for the acetylene cation," Nat. Commun. **5**(1), 4422 (2014).
21. T. Endo, S. P. Neville, V. Wanie, S. Beaulieu, C. Qu, J. Deschamps, P. Lassonde, B. E. Schmidt, H. Fujise, M. Fushitani, A. Hishikawa, P. L. Houston, J. M. Bowman, M. S. Schuurman, F. Légaré, and H. Ibrahim, "Capturing roaming molecular fragments in real time," Science **370**(6520), 1072–1077 (2020).
22. J. Pupeikis, P.-A. Chevreuil, N. Bigler, L. Gallmann, C. R. Phillips, and U. Keller, "Water window soft x-ray source enabled by a 25 W few-cycle 2.2 µm OPCPA at 100 kHz," Optica **7**(2), 168–171 (2020).
23. A. I. Gonzalez, G. Jargot, P. Rigaud, L. Lavenu, F. Guichard, A. Comby, T. Auguste, O. Sublemontier, M. Bougeard, Y. Zaouter, P. Georges, M. Hanna, and T. Ruchon, "Spatio-spectral structures in high harmonic generation driven by tightly focused high repetition rate lasers," J. Opt. Soc. Am. B **35**(4), A6–A14 (2018).
24. I. Sytcevich, C. Guo, S. Mikaelsson, J. Vogelsang, A.-L. Viotti, B. Alonso, R. Romero, P. T. Guerreiro, I. J. Sola, A. L'Huillier, H. Crespo, M. Miranda, and C. L. Arnold, "Characterizing ultrashort laser pulses with second harmonic dispersion scans," J. Opt. Soc. Am. B **38**(5), 1546–1555 (2021).
25. I. Sytcevich, A.-L. Viotti, C. Guo, J. Vogelsang, F. Langer, A. L'Huillier, and C. L. Arnold, "Few-cycle short-wave-infrared light source for strong-field experiments at 200 kHz repetition rate," Opt. Express **30**(15), 27858–27867 (2022).
26. X. Zhang, H. Fang, S. Tang, and W. Ji, "Determination of two-photon-generated free-carrier lifetime in semiconductors by a single-beam Z-scan technique," Appl. Phys. B **65**(4-5), 549–554 (1997).
27. J. Linnros, "Carrier lifetime measurements using free carrier absorption transients. I. Principle and injection dependence," J. Appl. Phys. **84**(1), 275–283 (1998).
28. J. Linnros, "Carrier lifetime measurements using free carrier absorption transients. II. Lifetime mapping and effects of surface recombination," J. Appl. Phys. **84**(1), 284–291 (1998).
29. A. Leblanc, P. Lassonde, S. Petit, J.-C. Delagnes, E. Haddad, G. Ernotte, M. R. Bionta, V. Gruson, B. E. Schmidt, H. Ibrahim, E. Cormier, and F. Légaré, "Phase-matching-free pulse retrieval based on transient absorption in solids," Opt. Express **27**(20), 28998–29015 (2019).
30. A. Longa, M. Kumar, P. Lassonde, H. Ibrahim, F. Legare, and A. Leblanc, "Spectral phase sensitivity of frequency resolved optical switching for broadband IR pulse characterization," Opt. Express **30**(5), 7968–7975 (2022).
31. A. Leblanc, A. Longa, M. Kumar, A. Laramée, C. Dansereau, H. Ibrahim, P. Lassonde, and F. Légaré, "Temporal characterization of two-octave infrared pulses by frequency resolved optical switching," JPhys Photonics **3**(4), 045002 (2021).
32. P. Lassonde, A. Laramée, H. Ibrahim, F. Légaré, and A. Leblanc, "Polarization-independent pulse retrieval based on frequency resolved optical switching," Opt. Express **29**(15), 23225–23233 (2021).
33. S. Gupta, M. Y. Frankel, J. A. Valdmanis, J. F. Whitaker, G. A. Mourou, F. W. Smith, and A. R. Calawa, "Subpicosecond carrier lifetime in GaAs grown by molecular beam epitaxy at low temperatures," Appl. Phys. Lett. **59**(25), 3276–3278 (1991).

Optics EXPRESS

34. F. Ganikhanov, G.-R. Lin, W.-C. Chen, C.-S. Chang, and C.-L. Pan, "Subpicosecond carrier lifetimes in arsenic-ion-implanted GaAs," Appl. Phys. Lett. **67**(23), 3465–3467 (1995).
35. J. Degallaix, R. Flaminio, D. Forest, M. Granata, C. Michel, L. Pinard, T. Bertrand, and G. Cagnoli, "Bulk optical absorption of high resistivity silicon at 1550 nm," Opt. Lett. **38**(12), 2047–2049 (2013).
36. J. M. Dudley, G. Genty, and S. Coen, "Supercontinuum generation in photonic crystal fiber," Rev. Mod. Phys. **78**(4), 1135–1184 (2006).
37. Y. Jee, M. F. Becker, and R. M. Walser, "Laser-induced damage on single-crystal metal surfaces," J. Opt. Soc. Am. B **5**(3), 648–659 (1988).
38. J. Bonse, S. Baudach, J. Krüger, W. Kautek, and M. Lenzner, "Femtosecond laser ablation of silicon–modification thresholds and morphology," Appl. Phys. A **74**(1), 19–25 (2002).
39. R. N. Oosterbeek, C. Corazza, S. Ashforth, and M. C. Simpson, "Effects of dopant type and concentration on the femtosecond laser ablation threshold and incubation behaviour of silicon," Appl. Phys. A **122**(4), 449 (2016).
40. C. S. R. Nathala, A. Ajami, W. Husinsky, B. Farooq, S. I. Kudryashov, A. Daskalova, I. Bliznakova, and A. Assion, "Ultrashort laser pulse ablation of copper, silicon and gelatin: effect of the pulse duration on the ablation thresholds and the incubation coefficients," Appl. Phys. A **122**(2), 107 (2016).